EUROPEAN FUSION DEVELOPMENT AGREEMENT

EFDA–JET–CP(02)01/16

M. Wischmeier, D. Coster, X. Bonin, T. Eich, A. Huber, C. Ingesson,
S. Jachmich, A. Kukushkin, A. Loarte, G. F. Matthews, R. A. Pitts,
J. Rapp, D. Reiter and E. Tsitrone

Divertor Detachment during Pure Helium Plasmas in EFDA-JET

Divertor Detachment during Pure Helium Plasmas in EFDA-JET

M. Wischmeier[1], D. Coster[2], X. Bonin[3], T. Eich[2], A. Huber[4], C. Ingesson[5], S. Jachmich[5], A. Kukushkin[6], A. Loarte[7], G.F. Matthews[5], R.A. Pitts[1], J. Rapp[4], D. Reiter[4], E. Tsitrone[8], and contributors to the EFDA-JET workprogramme*

[1]*Centre de Recherches en Physique des Plasmas, Association EURATOM-Conf dération Suisse, Ecole Polytechnique Fédérale de Lausanne, CH-1015 Lausanne, Switzerland*
[2]*Max-Planck-Institut für Plasmaphysik, EURATOM-Association, Garching, Germany*
[3]*Max-Planck-Institut für Plasmaphysik, EURATOM-Association, Greifswald, Germany*
[4]*FZJ-Forschungszentrum Jülich, Association Euratom-FZJ, Jülich, Germany*
[5]*UKAEA Fusion, Association Euratom-UKAEA, Culham Science Centre, Abingdon, UK*
[6]*ITER International Team, Garching Joint Work Site, D-85748, Garching, Germany*
[7]*EFDA-CSU, Max-Planck-Institut für Plasmaphysik, D-85748, Garching, Germany*
[8]*Association EURATOM-CEA, CEA Cadarache, 13018 St. Paul lez Durance, France.*
**See annex of J. Pamela et al., "Overview of recent JET results and Future Perspectives", Fusion Energy 2000 (Proc. 18th Int. Conf. Sorrento, 2000), IAEA Vienna (2001)*

Preprint of Paper to be submitted for publication in
Proceedings of the 15th PSI Conference, (GIFU, Japan 22-31 May 2002)

ABSTRACT

A campaign of pure helium discharges in the EFDA-JET tokamak equipped with the MarkII GB divertor has been performed. This paper describes some of the experimental observations of divertor detachment obtained in L-mode density ramp He discharges and presents a selection of results from the application of B2.5-Eirene code modelling to a JET He plasma. Detachment is very different from that observed in equivalent D discharges. Particle fluxes remain attached up to higher densities than in comparable D discharges. With decreasing input power, particle detachment occurs earlier in density, but the low measured target Te at all but the lowest ne, leads to an earlier decrease in power flux. Simulations show that detachment is caused by the escape of He neutrals from the target vicinity where, together with the He^+ ions, they radiate along the separatrix and above the X-point area starving regions downstream of power.

1. INTRODUCTION

A number of intimately linked key factors determine the onset and nature of tokamak divertor detachment, some related to magnetic and divertor geometry (parallel field connection lengths, degree of neutral baffling etc.) and many to details of distributed power loss in the divertor volume (momentum losses due to charge exchange and impurity and main plasma species line radiation). These volumetric losses are in turn governed by the material of first wall surfaces and the choice of fuelling gas. By exchanging deuterium for helium in a machine containing significant quantities of graphite, whilst retaining the important geometrical parameters, the effect on the character of detachment both of a significant change in both principal atomic physics processes and the nature of the carbon impurity source can be studied. Helium plasma discharges with helium neutral beam injection (NBI) and operating conditions matched to previous deuterium discharges have been performed during a recent EFDA-JET campaign in the MarkIIGB divertor configuration [1]. This paper concentrates on some of the key experimental observations of divertor detachment obtained in helium L-mode density ramp discharges and presents a selection of results from B2.5-Eirene code modelling of these pulses.

2. EXPERIMENT

The discharges discussed here are L-mode plasmas with I_p = 2.5MA, B_T = 2.4T, with strike points on the vertical divertor targets and are each characterized by a density ramp to the density limit with varying levels of He NBI power up to 5MW. The mean purity level of the He plasma discharges is around 90%, measured both by visible spectroscopy in the plasma edge and by monitoring partial pressures in the subdivertor volume. As shown in Fig. 1, these pulses have low wall clearance in the main chamber (similar density limit pulses in high wall clearance configurations are described in a seperate contribution to these proceedings).

Fig. 2 compiles the density dependence of key strike point experimental data from both target Langmuir probes and IR thermography for the inner (Fig. 2 (a - c)) and outer (Fig. 2 (d - f)) targets.

With the exception of the peak IR power (for which no data is available in D), the data are from three He discharges with varying P_{NBI} heating and a single D pulse for reference matched most closely to the He Pulse No: 4001, corresponding to the mid-range power in the heating scan. Note the considerably higher density limit in He compared with D [2]. Figure 2 shows clearly how the observed detachment in He is very different from that in D. At the inner divertor, particle (Fig.2 (a)) and energy (Fig.2 (c)) detachment occurs immediately in D. This is a common observation in JET discharges with the $B \times \nabla B$ drift direction towards the X-point [3].

In equivalent He plasmas, inner target ion fluxes begin to decrease at much higher densities, with the onset of detachment coincident with the formation of a strong X-point MARFE. This MARFE occurs earlier in density as input power is decreased. In common with D plasmas, Te at the inner target in He appears to be collapsed at all densities for the limited power scan described here (Fig.2 (c)). Note also the low peak powers (Fig.2 (b)), only just above the experimental sensitivity of the IR camera - although particles still arrive at the target, the energy flux is low.

At the outer target, particle flux detachment in He occurs at marginally higher $\bar{n}_e$ (Fig.2 (d)) in comparison with the inner target and is again sensitive to the degree of input power. In D for the reference case in fig. 2, the outer target remains attached almost until the density limit, where the formation of an X-point and then rapidly an inner wall MARFE occurs [2]. The outer target electron temperatures (Fig. 2 (f)) demonstrate clearly the effect of increasing input power and fall in He, as in D, to values of ~5eV as $\bar{n}_e$ increases. Unlike in D however, when Te falls in the He plasma, the particle flux does not (as also observed in the inner divertor). In D, strongmomentum loss is followed by recombination which ultimately decreases the particle flux [4]. Note that the known problems of Langmuir probe interpretation at low Te prevent any knowledge of the true value of Te at high [5]. In He, the peak IR power at the outer target (Fig.2 (e)) falls in synchrony with Te, despite the increasing ion flux (Fig.2 (d)).

Figure 3 illustrates the behaviour for a single case of the total radiation (from bolometry) and the He radiation light (HeI, 706nm, from inversion of tangential CCD camera images [6]) in the divertor as rises. Initially located at both the inner and outer strike zones at low $\bar{n}_e$, the total radiation increasingly concentrates at the inner leg and then finally above the X-point during the MARFE phase. Likewise, the HeI emission begins at the outer and switches to the inner at high $\bar{n}_e$. At high density in He, CIII emission in the divertor and main chamber is observed to extremely low levels. This is unlike the case in D, in which this emission remains constant or even increases with increasing [1, 2]. This is attributed to the absence of chemical sputtering in He and (and the decrease of ion energy below the threshold for physical sputtering at high $\bar{n}_e$) and implies that the radiated power (Fig. 3) in He is due almost exclusively to that from He^0 and He^+ at elevated densities.

3. SIMULATIONS

The SOLPS5 (B2.5-Eirene) code has recently been fully installed at JET and is now being routinely used for the simulation of D plasmas [7], however, modelling the complex high density detached

cases has only just begun and the results are insufficiently mature to be included here. In helium, the absence of hydrocarbon chemistry and molecular species renders the situation somewhat less complex. The basic findings reported here have much in common with those found in an earlier attempt at He plasma modelling [8] for DIII-D discharges with the older, SOLPS4 version of the code. The latter has also been used to simulate a single reference JET He plasma case and the results found to be in good agreement with those of SOLPS5 reported below. The simulations are conducted on a grid (Fig.1b) extending from $\rho = -4$cm to $\rho = 3$cm in outer midplane coordinates - chosen so as to be compatible with concurrent EDGE2D-NIMBUS and UEDGE [8] modelling of similar discharges. Radial transport coefficients $D_\perp = 0.2\ m^2\ s^{-1}$, $\chi_\perp = 0.2\ m^2\ s^{-1}$ are used in these first simulations - sensitivity studies to variations in these coefficients are underway.

Ion sputtering occurs only at the divertor targets in SOLPS5, whilst neutral interaction with divertor and main chamber walls is included in the model. Physical sputtering is implementedaccording to the Roth-Bodansky formula [9] with chemical sputtering (for the D minority) fixed at 1%. Concerning the percentage of D in these code runs, sensitivity tests have been performed for constant n e and input power P_{SOL} at the inner boundary of the simulation grid by varying the ratio of density due to D^+ and He^{2+} ions corresponding to D concentrations up to 40%. No significant change in the target profiles was observed throughout this concentration scan, in contrast to the findings for SOLPS5 simulations with horizontal target geometry [7]. This apparent sensitivity in the code to divertor geometry is the subject of ongoing study. For the results presented here, the D concentration was fixed at values below 8%.

For fixed $P_{SOL} = 3.8$MW, comparable to Pulse No: 54001 of Fig.2, fig. 4 compiles code output and target probe measurments for n_e, Te and ion particle flux profiles across the outer and inner targets mapped to the outer midplane. Code output is plotted for 6upstream separatrix densities in an attempt to simulate the experimental density ramp. The probe data for all densities in the ramp is included to indicate the spread in the experimental results. Agreement is in general reasonable given that transport coefficients have been fixed for code optimization and code comparison rather than providing the best match to upstream profiles, although there is a persistant tendency in the code to underestimate Te in the strike point and private flux regions at all but the lowest densities.This does not appear to be the case for compareable UEDGE and EDGE2D simulations in which Te is well matched at the outer target, though none of the codes (drifts are not included) can match the inner/outer target asymmetries seen in experiment. Further SOLPS5 simulations are planned (variation of transport coefficients, P_{SOL} etc.) in order to investigate this interesting discrepancy further.

Of note in fig. 4 is the collapse of target and upstream separatrix densities as the inner boundary density reaches $n_e^{inn} = 4 \times 10^{19} m^{-3}$ in the code. In Fig.5 the variation with n_e^{inn} of total ion and power flux to the targets with shows that the general observation (Fig. 2) in Helium of power flux detachment before particle loss is reproduced by the code. The simulations also demonstrate a tendency for lower total power flux to the inner target compared with the outer.

In the context of this study the principle differences between He and D are the increased mean-free-path for neutral ionisation ($\lambda^{He}_{mfp} \sim 6\lambda^{D}_{mfp}$ at 10eV) and the reduced CX reaction rates (factor of 3-4 at 10eV). What happens is simply that neutral He recycled at the targets penetrates further upstream before being ionized than would be the case for D neutrals. Figure 6 illustrates this effect from the point of view of the code. With increasing $\bar{n}_e$, the ionisation fronts for He^0 and He^+ move progressivly further away from the targets to produce a strong radiating zone dominated by HeII line radiation starving the divertor of power until pressure collapse prevents further ionisation and the target flux falls.

The main carbon sputtering mechanisms in these simulations are physical sputtering due to He+ and He^{2+} ion impact, although D and D+ contribute to the total sputtered flux at levels up to 30% due to the observed (in the simulations) accumulation of D+ ions in the divertor region. At high densities, this contribution can amount to 25% of the total electron density in the target region. With increasing n_e^{inn} the total carbon content in the simulations decreased by a factor of approx. 2 (the ion fluxes always remaining negligible compared to the He ion fluxes at the targets), and the radiative losses due to CIII and CIV, reaching their maximum only at the lowest simulated densities, are always low (2% to 25%) compared to these losses from HeII.

Similar simulations for Pulse No: 53088 are under way and extensive comparisons will be done in the future.

4. DISCUSSIONS AND CONCLUSIONS

In helium, divertor detachment begins at much higher upstream densities than in deuterium and is similar to that in deuterium at most in the sense that the inner target detaches first. For varying input power, only at the highest densities, at high input power, particle detachment is observed at both targets. Particle detachment occurs close to the density limit whilst power detachment is observed to occur at much lower densities. From comparison of simulations and experimental data it is clear that the power detachment is a consequence of He atoms escaping further upstream compared to the case for D neutrals followed by power loss due to He^+ line radiation. At the highest densities a large enough fraction of the power entering the SOL is lost through HeII line emission that there is insufficient energy for ionization of the recycled neutrals, thereby leading to a collapse in particle flux to the targets. This is very different to D plasmas where a complex interdependence between CX reactions, radiative cooling due to high carbon concentrations, recombination and ionization processes lead to the observed power and particle detachments. In He, recombination processes play no role during detachment since insufficient momentum is removed by ion-neutral friction to allow confinement times for He^+ in the divertor region to recombine effectionally. Due to the few simple atomic key processes involved in the detachment of He plasmas (and the absence of molecular species) they are an ideal subject for bench marking SOL codes. It is not yet clear why e.g., for vertical targets with the MarkII GB divertor, B2.5-Eirene produces very low electron temperatures in the strike point and private flux regions compared to higher values simulated by UEDGE and EDGE2D-NIMBUS and measured by target Langmuir probes. A comparison with SOLPS5 simulations for a matched JET deuterium discharge is under way.

ACKNOWLEDGEMENT

This work was performed under the European Fusion Development Agreement and was supported in part by the Swiss National Science Foundation, EURATOM and the UK Department of Trade and Industry.

REFERENCES

[1]. R. Pitts et al., these proceedings (PSI-15)
[2]. J. Rapp et al. , these proceedings (PSI-15)
[3]. G. McCracken et al., J. Nuclear Mater., **266-269** (1999) 37
[4p]. P. C. Stangeby, The Plasma Boundary of Magnetic Fusion Devices, IOP (2000)
[5]. J. Horacek et al., these proceedings
[6]. A. Huber et al., these proceedings (PSI-15)
[7]. D. Coster, these proceedings
[8]. M. Fenstermacher, these proceedings (PSI-15)
[9]. A. Loarte, Contrib. Plasma Phys., **40** 3-4 (2000)
[10]. Roth, J., Gracia-Rosales, C., Nucl.Fus. **36**, 12, (1996), 1647

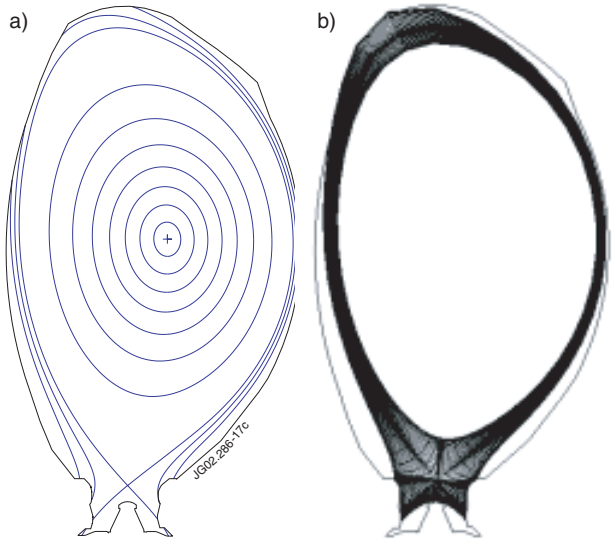

Figure 1: a) JET high clearance equilibrium referred to in this paper and the grid (b) used in the simulations.

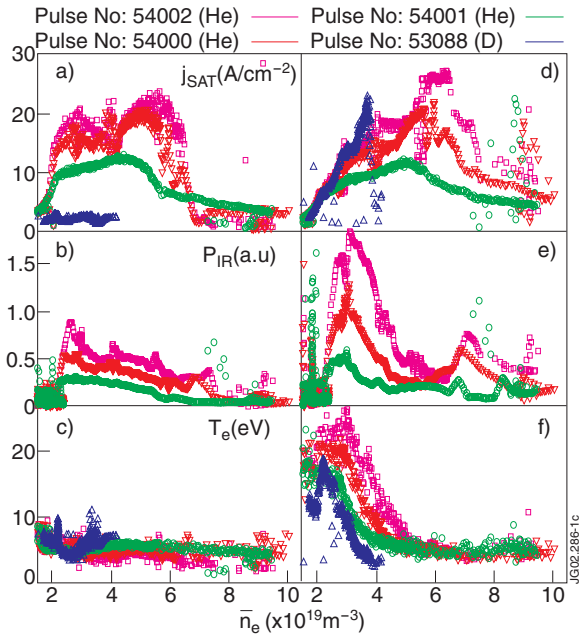

Figure 2: (a, d) electron density, (b, e) IR peak heat flux, (c, f) electron for inner (left column) and outer (right column) target for #53088 (D), He #54000, #54001 and #54002

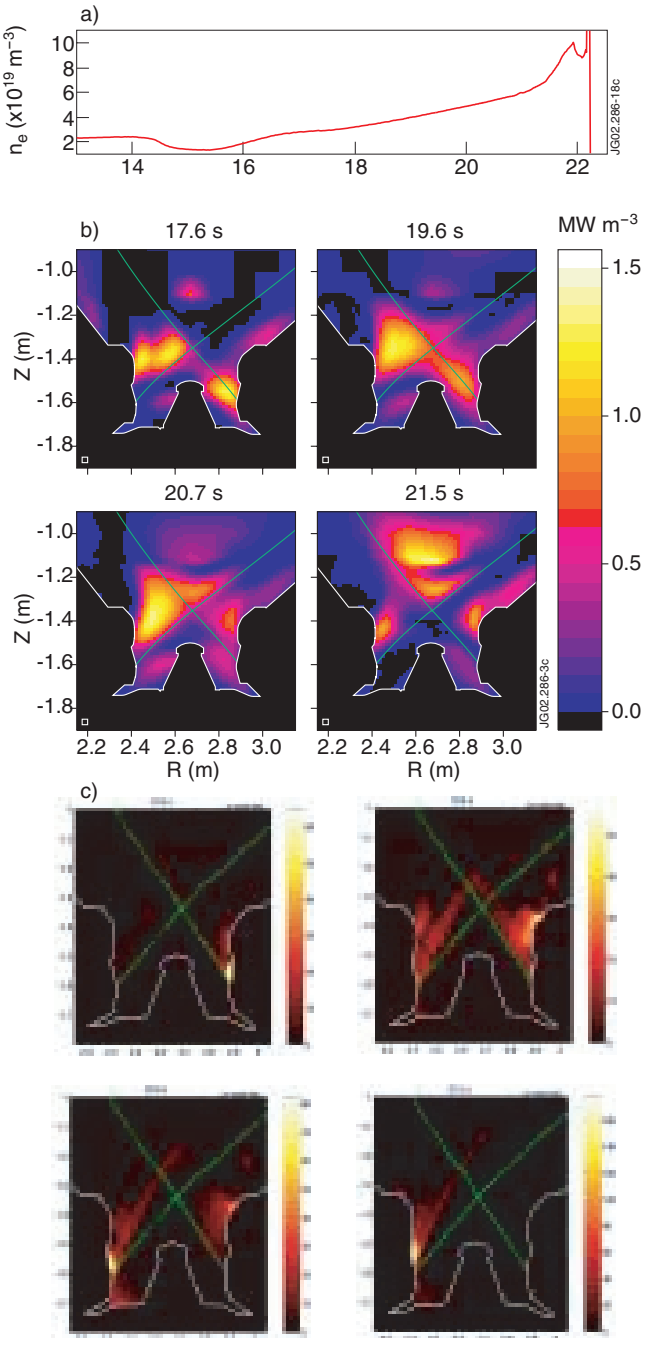

Figure3: a) Time trace of density ramp for #54001; b) bolometric inversions and c) in-versions from KL1 for He^0 at 706nm for the four indicated times. The HeI light is tomographically inverted from the 2D emission distribution of a filtered tangential CCD camera view of the divertor

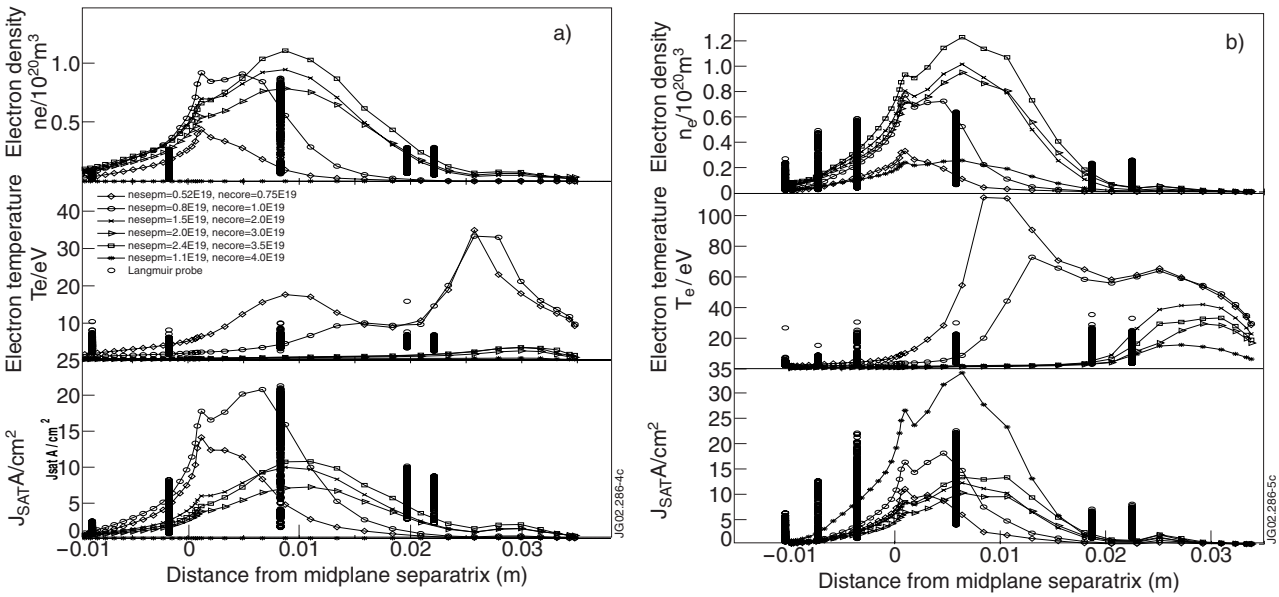

Figure 4: Comparison of simulated electron density, electron temperature and saturation current with data from Langmuir probes during density ramp up in #54001 after the formation of the divertor. Data are mapped to the outer midplane. a) inner divertor, b) outer divertor

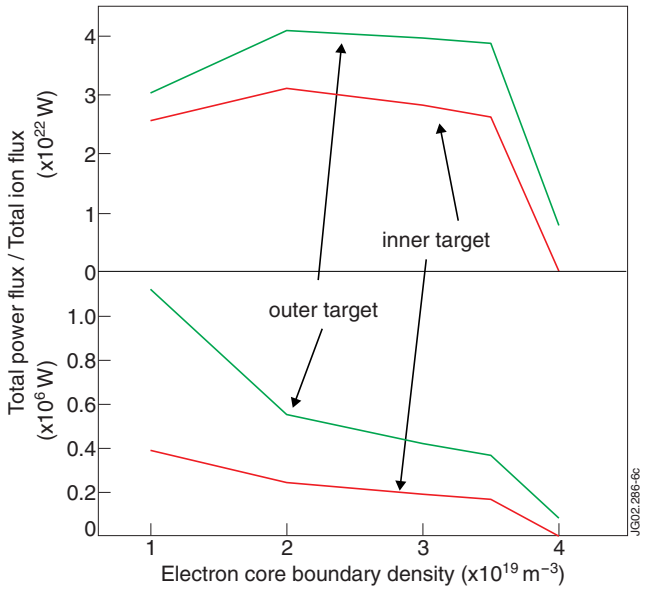

Figure 5: Total simulated ion flux and power flux to the inner and outer targets

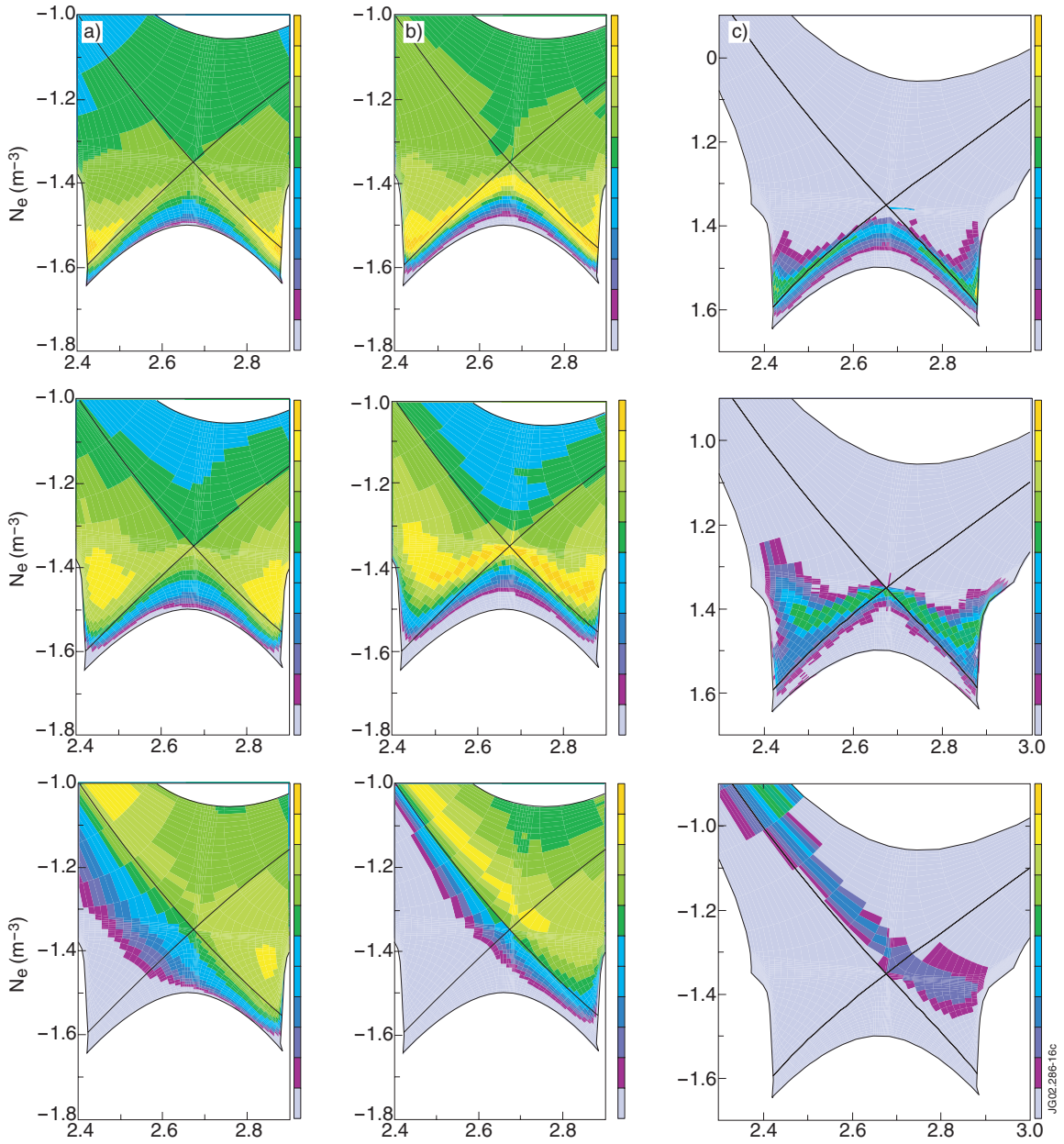

Figure 6: Dependence of the movement of the ionization front for He (a) and He^+ (b) and of the total radiation (c) with density (rising from top to bottom) in the simulations